Theoretical Design and Manufacturing of a UAV for Delivering Relief Material

Anuj Kumar[1], Bibek Agrahari[2], Sachin Bucha [3]

[1]*Department of Aerospace Engineering, Lovely Professional University, Phagwara, Punjab, 144001, India.*
[2,3] *Undergraduate student, Vel Tech Rangarajan Dr. Sagun Thala R&D Institute of Science and Technology University, India*
Anujkumarx117@gmail.com[1] ,*bivekagrahari124@gmail.com*[2] ,
buchasachin@gmail.com [3]

Abstract:

Unmanned aerial vehicles (UAVs) can revolutionize the medical industry's last-mile delivery segment. UAVs can supply necessary goods, especially in isolated and difficult last-to-reach locations. The papers explore design methodology that can be used to design UAVs suited for the prompt and effective delivery of medical goods. We have focused on calculating aerodynamic parameters, structural calculations, and performance parameters like range and endurance for designing this UAV. To better calculate aerodynamic parameters, we have used open-source CFD, which has acted as design verification and validation for the design. The results will be used as a milestone in designing and developing UAVs for medical deliveries.

Keywords*: Aircraft, UAV, Aerial cargo, Open Foam, XFLR5, FEA*

Nomenclature:

S_w	Wing Span
Cr	Root Chord
Ct	Tip Chord
AR	Aspect Ratio
TR	Taper Ratio
c_{mean}	Mean Aerodynamic Chord
Cl_{max}	Maximum Lift Coefficient
Clc	Cruise lift Coefficient
Cdo	Drag Coefficient at Zero Angle of attack
Lf	Fuselage Length
lopt	Tail arm
$Cl_{required}$	Required Lift Coefficient
Cdmin	Minimum drag Coefficient
$\frac{Cl}{Cd}$	Lift-to-drag ratio
Clm	Lift Curve Slope
Aw	Wet Area
C_m	Lowest pitching moment coefficient
Re	Reynolds Number
C_n	The moment around the yaw axis
Cl	The moment around the Roll axis
mAh	Milliampere hour
CFD	Computational fluid dynamics
CAD	Computer-Aided Design
RAS	Reynolds-Averaged Simulation

AoA	angle of attack
ø	roll angle
α	angle of attack
β	sideslip angle
θ	pitch angle
φ	yaw angle

1. Introduction:

Drones, also known as UAVs (unmanned aerial vehicles), are aircraft piloted remotely or by themselves. These nifty machines can carry gadgets like cameras and sensors, along with other payloads. They come with a handy autopilot feature, allowing them to handle multiple tasks on their own a feature that makes them super useful for certain jobs[1]. Are you aware that drones took their first flight during World War I [2] Thanks to the rise of TV and radio back then, these crafty UAVs were created to take down Zeppelins with grand results. As the nineties came to a close, drones started to carve out their place in warfare. However, the technology was quite pricey and was mostly found in military circles. Now, with recent leaps in tech, the drone market is booming and spreading its wings into new areas. UAVs are used for tons of things now like spying from the air, helping farmers, studying the environment, making deliveries, and even fighting battles. Let's zoom in on one use of delivering aid to people stuck in hard-to-reach areas. Quick, on-point, and effective responses are essential when disasters strike, whether caused by humans or nature. Since these hit spots are often out of reach, we need ways to gather info and deliver aid to those affected before the main help arrives. That's where drones come in [3]. We'll be talking about a drone type called fixed-wing UAVs. They're a favorite for mid to long-distance missions whe-re heavy loads are involve-d, thanks to the lift generate-d by their wings during flight[4]. Because of the-se traits, fixed-wing drones make- sense for missions that call for fast speeds, vast distances, and significant flight times [5]. The go-to setup is a single rotor with a standard tail design. Most of these- jobs are tackled by a group of small (mini) UAVs, either flying solo or with remote guidance. Their usual specifications are Low altitude, a cruising speed between 30 100km/h, able to fly up to 500 m high, lightweight, and capable of operating in all we-ather conditions. These small drones typically have a wingspan of 1-2 m and can fly even if they weigh less than 25kg [6–8]. As with any system, they must be reliable, useful, and operational. The present work intends to investigate the design, performance, and realistic programs of fixed-wing UAVs in catastrophe relief situations. By studying case research and present-day deployments, we intend to focus on the strengths and limitations of those drones. Furthermore, advancements in battery generation, substance science, and AI-driven navigation structures are poised to decorate the skills of constant-wing UAVs even similarly, making them vital gear in diverse fields. In conclusion, the flexibility and growing affordability of drones, in particular constant-wing UAVs, are reworking more than one industry. From saving lives in disaster-bothered regions [9] to optimizing agricultural practices, these unmanned aerial cars are proving to be innovative. As generation continues to strengthen, we can expect even extra innovative and lifestyle-changing applications for drones in the destiny[10]. The key objectives of this study can be summarized below.

- To design and develop a low-cost fixed-wing UAV design.
- A brief overview of aircraft design methodologies that can be adopted for UAVs to reduce the R&D cost.
- Using open-source tools eliminates the need for commercial software, thus again saving the cost of design and analysis.
- The following work will be used as a benchmark for future design and optimization work by the authors.

2. Methodology:

We can distinctly categorize the aircraft design process into three phases: Conceptual, Preliminary, and detailed design [9]. The conceptual design phase is where you decide on basic mission constraints defined by customer aircraft configuration required to satisfy such constraints. The preliminary design phase is categorized by low-fidelity CAD/CAE simulation to estimate the selected design's aerodynamic performance and structural requirements. In Conceptual design, we go through different aircraft concepts and design spaces. It also includes trade studies that establish a balance between two or more constraints/requirements[11]. The preliminary design phase includes further refinement of selected concepts, like finding improvements, assessment of performance, and several low-fidelity analyses and tests. Detail design is where we start looking at how the aircraft fabrication processes, and testing of major subsystems like landing gear, and structure. Finalization of weight and performance estimation also comes under this phase. A linear approach has been used for designing the UAV, which begins with defining the constraints and calculating the Parameters, which are then used to create a CAD model followed by analysis/simulation. The CAD model will be used in Open FOAM simulations to validate the required performance. The design methodology can be validated through physical testing[12]. Apart from aerodynamic characteristics, we can also test the strain in different parts using methods such as strain guages[13]. Readers can refer to [14] for the design methodologies of an unmanned aerial vehicle.

2.1 Design Constraints:

For initial estimates of aircraft design parameters, these are the constraints that we will look at.

- The entire UAV can be stored in a 1.4m x 1m x 1m box after disassembling.
- Should be cost-effective and affordable.
- Can belly land to deliver cargo to inaccessible places.
- Should offer a payload capacity of more than 450 grams.
- A Pusher-type configuration is better if we want to avoid the propeller from being damaged during landing.

2.2 Aircraft configuration:

Aircraft are going to be primarily used for delivering medical cargo, so we have to make them reliable, durable, cost-effective, and easy to handle. To satisfy these criteria, we explored original designs like V-tail, H-tail, Cruciform-tail, and Tail. A design with an H tail was finalized, because of the following reasons.

1. This vertical tail has higher performance if they are in the prop wash region in a multi-engine turboprop. The vertical tail also increases the aerodynamic efficiency of the aircraft's tail [15].
2. The H-tail allows the twin vertical tail span to be shorter [6], for storage aboard an aircraft carrier, where space is limited
3. The lateral control of the aircraft will be enhanced because of a smaller vertical tail span
4. The H-tail allows the fuselage to be shorter since the entire tail is on the boom [6], but conventionally, the H-tail is considered being slightly heavier than other configurations, too.

2.3 Airfoil Selection and Initial Sizing

2.3.1 Airfoil selection:

Xflr5 was used to analyze different airfoils, performance was the key criterion for selection. The airfoil selection depends on aircraft requirements [16]. For simplicity, we will look at the following parameters to select an airfoil for maximizing aircraft performance [17].[6, 18, 19] Can provide a decent overview of airfoil selection.

1. Maximum lift coefficient C_{Lmax}
2. Lowest minimum drag coefficient C_{dmin}
3. Highest lift-to-drag ratio
4. Highest lift curve slope
5. Lowest pitching moment coefficient C_m

And for maximizing the range and glide performance, we have two criteria to fulfill.

1. We know that $\frac{C_l}{C_d} = \tan\gamma^{-1}\gamma$ being the glide angle. This means that a high $\frac{C_l}{C_d}$ is crucial for a long glide distance [17].
2. On the other hand, the sailplane's sink speed is given by

$$Vs = \frac{C_d}{C_l^{3/2}} \sqrt[2]{\frac{2*w}{\rho s}} \quad (1)$$

Therefore, a high $\frac{C_l^{3/2}}{C_d}$ factor is important for a long flight [16].

3. The Aerofoil should exhibit high C_{lmax} and low Cm to promote stability and decrease drag, with the lowest drag [17].

A comparison graph of lift and the drag coefficient is given in Fig. 1 FX 67-K-150/70 has the highest value of C_l At angles smaller than 10 deg and larger than 5 deg, whereas RG-15 has the lowest drag coefficient. The moment of coefficient is given in Fig. 2, where we can see that RG-15 has the lowest moment of coefficient at 0 deg.
Talking about the lift-to-drag ratio given in Fig. 3, FX 67-K-150/17 has the highest value between 5 and 10 deg angle of attack, the same thing applies to $\frac{C_l^{\frac{3}{2}}}{C_d}$ The aerofoil FX 67-K-150/17 was chosen. This aerofoil has a nice thick chamber, big enough to fit the wing's spar and reinforcement rods. The airfoil parameters are given in Table 1. This airfoil can further be optimized using the methodologies given in [20, 21].

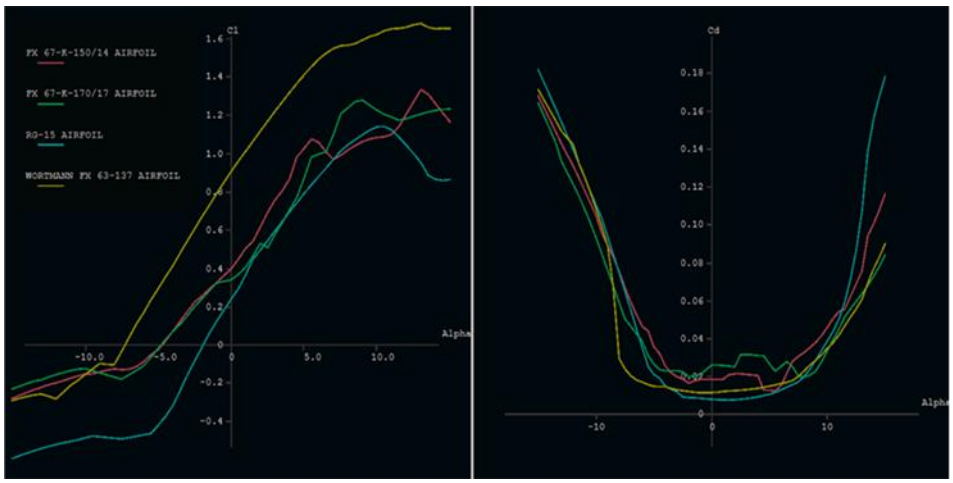

Fig. 1 Graph of Cl and Cd obtained from XFLR5

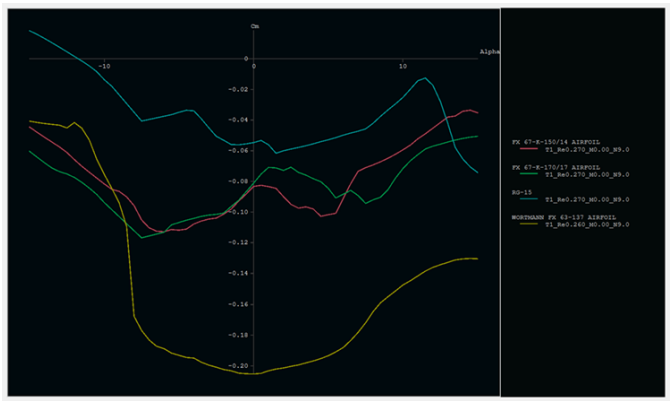

Fig. 2 Coefficient of moment (C_m) Graph

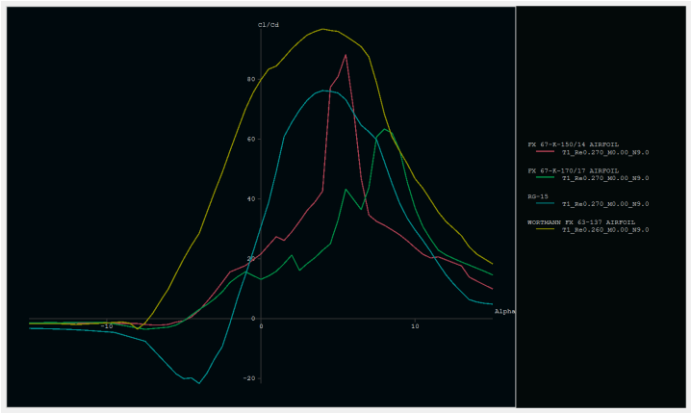

Fig. 3 Lift-to-drag ratios

For horizontal stabilizer, NACA 0012 was preferred and for vertical stabilizer, NACA 0009 was finalized because the Lift coefficient and coefficient of the moment were in a satisfied range. Airfoil can be optimized in the future to yield a boost in aircraft's performance as given in [21].

Table 1 Airfoil Parameters

Parameter	Symbol	Value
Max lift coefficient	C_lmax	1.1
Zero drag lift coefficient	C_d0	0.037
Zero lift angle	α_(C_l=0)	-4.628
Reynold number	R	220,000
Parameter	Symbol	Value
Max lift coefficient	C_lmax	1.1

2.3.2 Wing and tail design:

For smaller airplanes, a wing loading off $\frac{20\ \text{oz}}{\text{ft}^2}$ would give us a stall speed of $31mph$ as given in [6, 16]. We can find the area required for the wing using this formula

$$\text{area} = \frac{\text{weight(oz)*144}}{\text{wing loading (oz/ft}^2)} \quad (2)$$

Note the above formula provides an area in inches. The equation used to calculate the geometric parameters of the wing and tail are given in [6]. The final parameters are given

in Table 2, Table 3, Table 4. The design of control surfaces has not been shown in the study, one can refer to [22] for understanding the hinge moments of different control surfaces. Based on which sizing can be carried out.

Table 2 Wing Parameters

Parameter	Value	Unit
Span	1.32	m
Area	0.235145	m2
Root chord	0.238359	m
Tip chord	0.095344	m
Incidence Angle	4	deg
Aspect Ratio	7.5	
Tapered Ratio	0.4	
Dihedral	0	deg
Mean Chord	0.177	m
Max Lift Coefficient	1.22	
Cruise Lift Coefficient	0.423	
Incidence angle	3.5	deg
Sweep	3	deg

Table 3 Horizontal Tail Parameters

Parameter	Value	Unit
Area	0.0328	m^2
Span	0.41	m
Root chord	0.0811	m
Tip chord	0.0811	m
Fuselage length	0.7726	m
Moment arm	0.5022	m
Required Lift coefficient	-0.221	

Table 4 Horizontal Tail Parameters

Parameter	Value	Unit
Area	0.153	m2
Span	0.152	m
Root chord	0.131	m
Tip chord	0.0654	m
Tapered Ratio	0.50	
Aspect Ratio	3	

2.3.3 Preliminary Aerodynamic Calculation:

The preliminary aerodynamic calculation is the next stage in aircraft design after knowing the specifications in the conceptual design phase. This phase includes the evaluation of aircraft performance in terms of its aerodynamic performance, and stability requirement [23]. For this NASA's open-source software, OpenVSP [24] will be used. To obtain preliminary aerodynamic data and stability data, the aircraft model will be simulated in OpenVSP. The resulting geometry will be used with Open FOAM for final aerodynamic calculation and optimization. The final view of the design is given in Fig. 4.

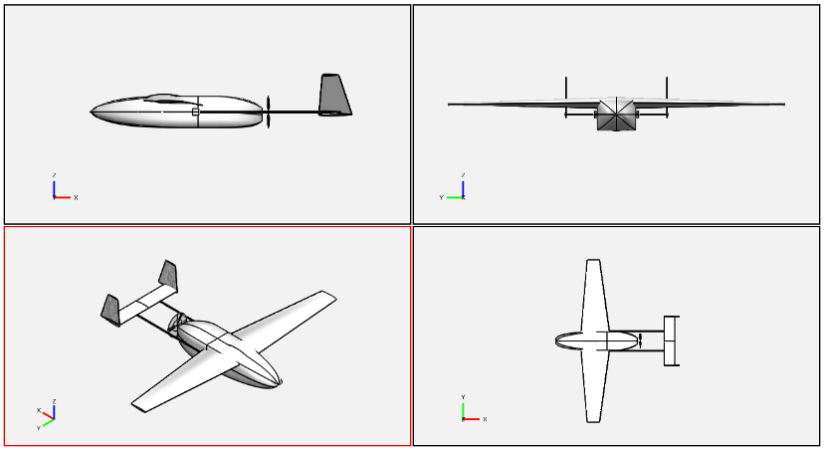

Fig. 4 First angle projection of the Design

After completing the geometric modeling, VSPAERO was used to perform some preliminary analysis using the vortex lattice method[25]. The lift distribution of the design was calculated, which was used to optimize the wing and tail plan form.
We also calculated parasite drag (combination of form drag and skin friction drag) of the entire design, along with the contribution of each design component. This helped us to optimize the fuselage shape further. Final data is given in Table 5.

Table 5 Parasite drag estimation

Component Name	$Swet\ (mm^2)$	Cd	Total
Connector x2	9525	0.000148	0.719238
Rod x2	1825	0.000647	3.147925
Horizontal Stabilizer	71723.14	0.001924	9.353689
Vertical Stabilizer	62640.51	0.001565	7.611095
wing	425584.82	0.010453	50.82138
Fuselage	276207.07	0.005035	24.47951
Geometry Total	4834.59656	0.020568	100

2.4 Stability analysis:

For analyzing and optimizing the stability of the design, the XFLR5 program [26]was used. Based on the outputs of XFLR5 location of various components will be determined along with geometrical parameters like fuselage length. The first step was making the plane statically stable and ensuring dynamic stability.The stability criteria is derived from [27] which talks about airplane flight Dynamics and Automatic Flight Controls.

2.4.1. Static stability:

The neutral point was calculated at 101.5 mm from the wing's leading edge, and a static margin of 15 percent was taken, which resulted in a CG to be at 75 mm from the wing's leading edge. Static stability is defined as the tendency of an aircraft to return to its equilibrium state when disturbed.[23, 28] gives a summary of the methodology that we have adopted for stability analysis.

- Longitudinal stability: For an aircraft to have longitudinal static stability, its tail should produce a pitching moment to cancel the moments produced by the aircraft. When the aircraft dives (because of disturbance) tail produces a pitching up moment, in case of climb (because of disturbance) a pitching down moment is produced [6] in Fig. 5, one can observe the variation in C_m concerning the Angle of attack needed for a stable design.

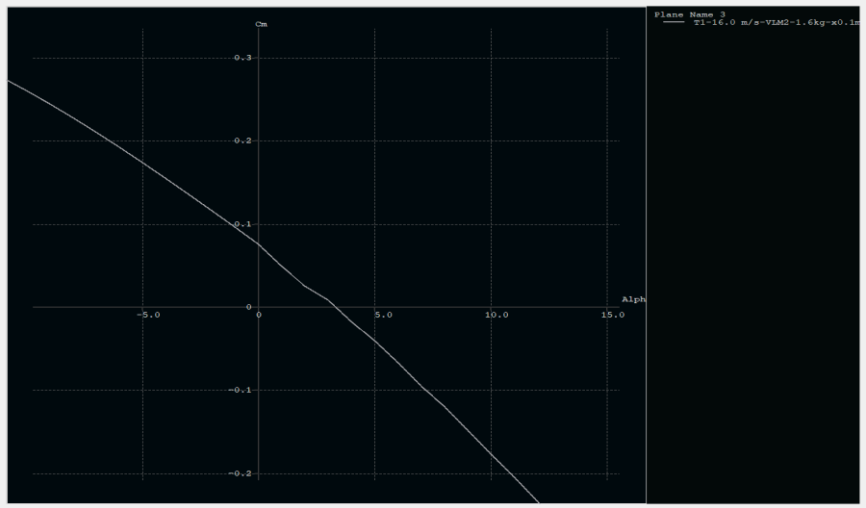

Fig. 5 Aircraft pitching moment coefficient along the aircraft's lateral axis.

- Directional static stability: For an aircraft to be directionally stable, its tail should be able to produce a restoring yawing moment to cancel the yawing moments produced in the aircraft created because of disturbance. The restoring moment should be produced along the Normal axis of the aircraft as shown in Fig. 6.

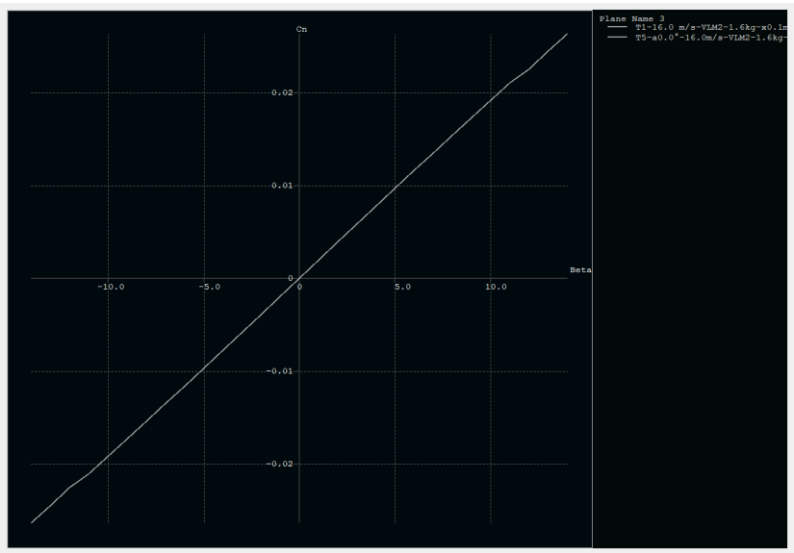

Fig. 6 Aircraft yawing moment coefficient along normal axis

2.4.2. Dynamic stability:

An aircraft's dynamic stability can be understood as the tendency to dampen the motion induced because of any disturbances. From the mathematics point, these disturbances are dubbed as modes and they are described by an eigenvector (the modal shape) and

Eigenvalue (frequency of mode and its damping). Eigenvalue can be understood in the sense of these two parameters: the period required for one complete oscillation, and the time required to damp to half-amplitude. A well-designed plane will have 4 natural longitudinal modes[29, 30] and 4 natural lateral modes. These are given in Table 6**.**

Table 6 Dynamic Stability Modes

Longitudinal mode	Lateral modes
Two Symmetric Phugoid modes Two Symmetric short-period modes	Spiral mode Roll damping mode Two Dutch roll modes

Phugoid, Short period, and Dutch roll modes are oscillatory [30]. When the aircraft is in the air, disturbances such as sudden control input or a wind gust will excite all the modes. Responses of short-period mode and roll damping are quick, and not noticeable by human eyes. Whereas responses of Phugoid and Dutch roll modes are visible to human eyes. All the modes are damped well, except for spiral mode, which will be damped using user controls.

- Short period mode: In short period mode there is primarily a vertical movement along with some pitch rate in the same phase, usually high frequency, in Fig. 7 we can see that this mode is well-damped for our design. This mode's behavior is defined by the stiffness of the negative slope of the curve.

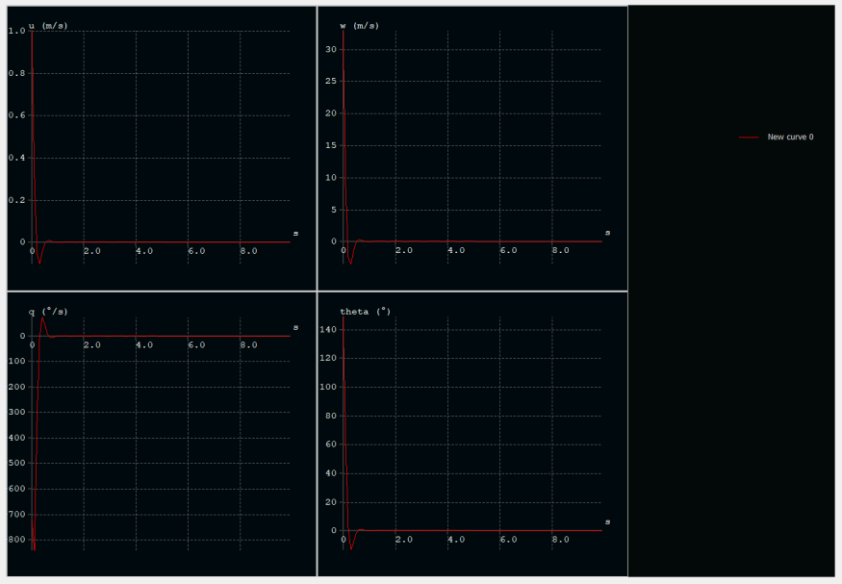

Fig.7 Short Period Modes

- Phugoid modes: Phugoid mode is defined as the mode of exchange between the Kinetic and potential energies. When a plane dives because of reduced lift, it accelerates which increases the lift generating a pitch moment, so the entire aircraft will pitch up. This will repeat, so it needs to be dampened effectively. In Fig. 8, we can see that this mode is effectively damped in our design.

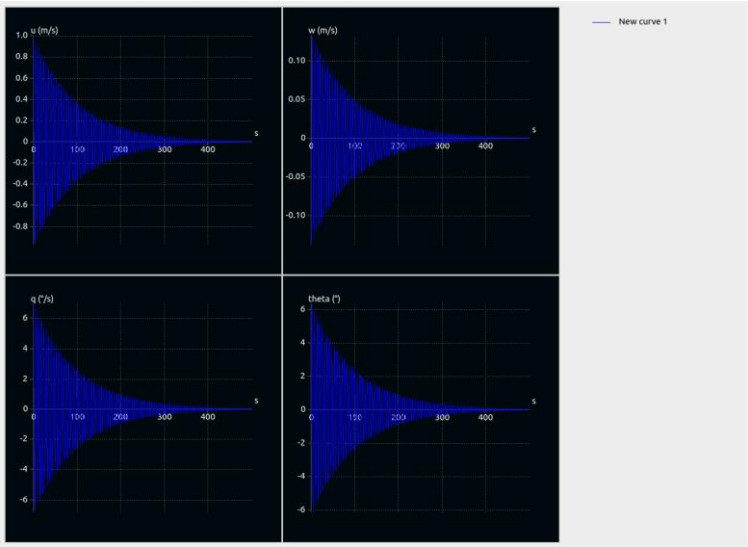

Fig.8 Phugoid Mode

- Roll damping: when we have a roll about the aircraft's longitudinal axis, the wing coming down will experience an increase in Aoa, thus increasing the lift on that side. Because of the symmetry, a decrease in lift will be experienced on the other end of the wing. This will generate a restoring moment opposite to the roll, which will dampen the mode. The roll damping of the design is shown in Fig. 9

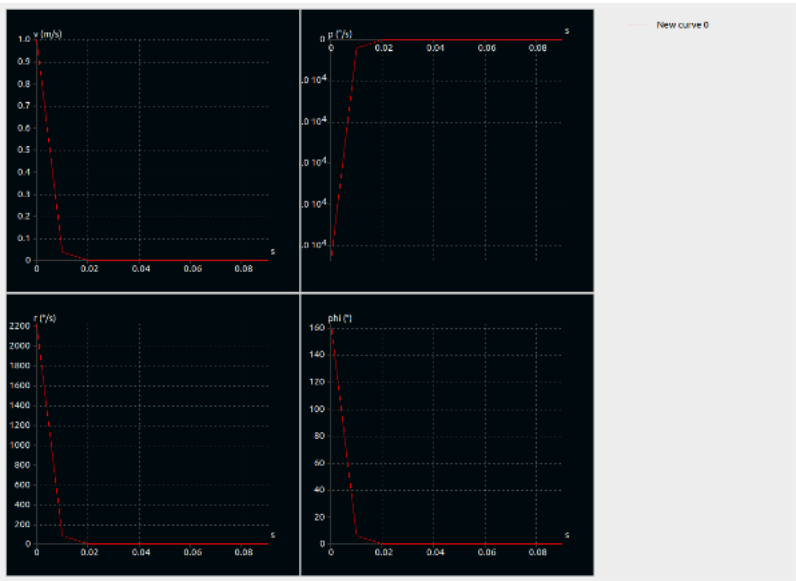

Fig. 9 Roll damping mode

- Dutch Roll: In Dutch roll mode, we see a combination of roll and yaw phased at 90 deg, usually lightly damped.One can notice the nature of Dutch roll mode from Fig. 10.

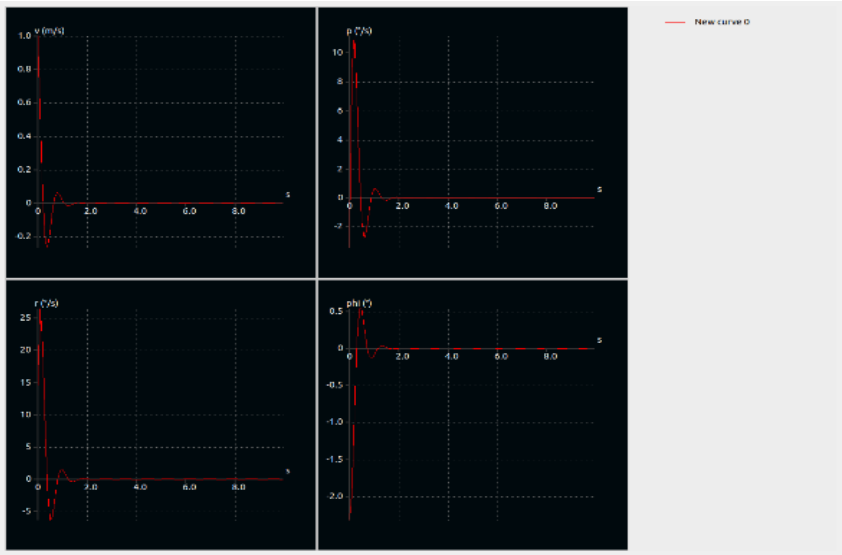

Fig. 10 Dutch roll

- Spiral mode: This model is non-oscillatory as shown in Fig. 11 and slow, usually requiring pilot input for correction. The mode is initiated because of a rolling or heading disturbance, which creates a positive AoA on the fine, increasing the yawing moment.

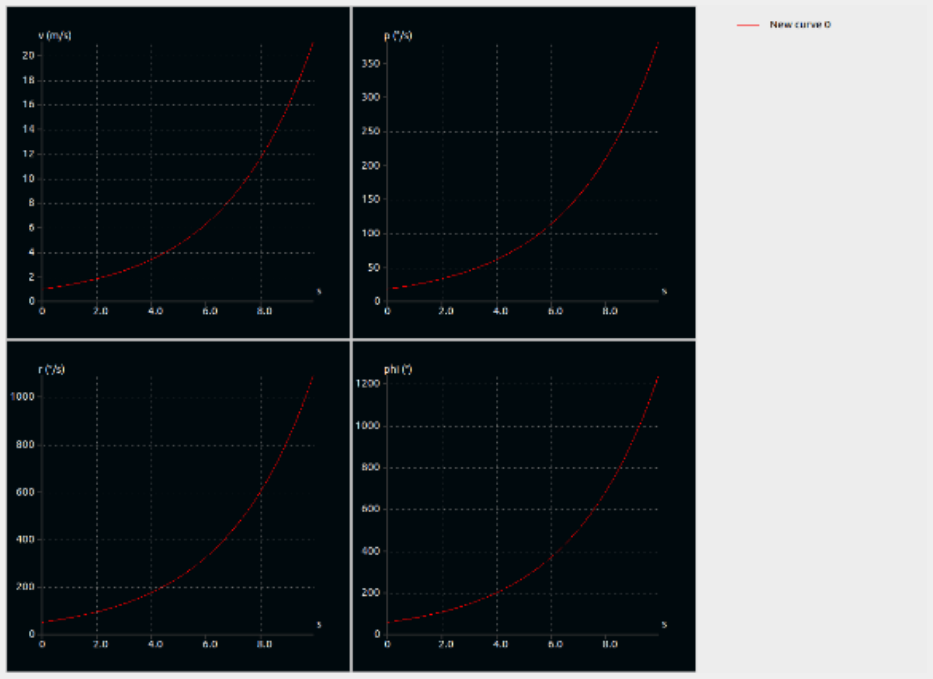

Fig. 11 Spiral mode

2.5. Technical data:

Here is data about the moment of different components of the aircraft. All the readings were taken from xflr5. Table 7 is for loaded cases and it contains the weight data of every component in the aircraft. The final CG is closer to 75mm from the nose.

Table 7 Analytical Moments

S.No.	Part Name	Weight(grams)
1	payload	500
2	battery	148
3	battery 2	148
4	fuselage	387
5	wing	345
6	tail	50
7	Tail servo	36
8	aileron servo	24
	total	1638

4. High Fidelity Aerodynamics:

The section contains the results of the final aerodynamic simulation. This simulation was completed in OpenFOAM, which is an open-source CFD package. The OpenFOAM (Open Field Operation and Manipulation) CFD toolbox is an open-source CFD package with tremendous community support expanding over major areas of engineering[31]. OpenFOAM comes packed with 80 solvers which can be expanded by the users. OpenFOAM can perform pre-processing (meshing) and post-processing tasks (data visualization). Above all, OpenFOAM will let you take full advantage of your computer hardware[32, 33].

4.1. Meshing and solver setup:

Mesh was generated in the snappyHexMesh utility [34]. Fig. 12 shows a snapshot of the generated mesh.

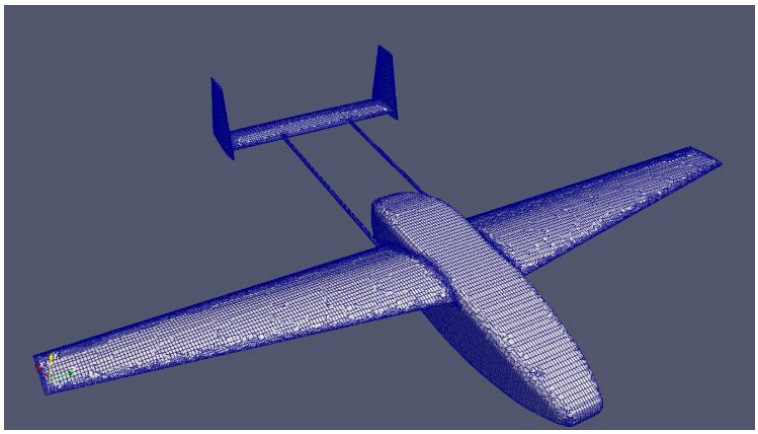

Fig. 12 Mesh generated using snappyHexMesh

The model uses an incompressible flow solver [32, 35] that is Simple Foam. The flow velocity is 17m/s.

4.2. Results:

For calculating lift and drag coefficients, the following equations were used.

$$C_l = \frac{L}{q.s} \quad (3)$$

$$C_d = \frac{D}{q.s} \quad (4)$$

Where L and D are the lift and drag per unit span, q is the flow dynamic pressure, and so is the wing area. Dynamic pressure q is defined as $\frac{\rho v^2}{2}$, where ρ is the fluid density, and v is the free-stream velocity[36–38]. Fig. 13 and Fig. 14 show the pressure contour and flow lines.

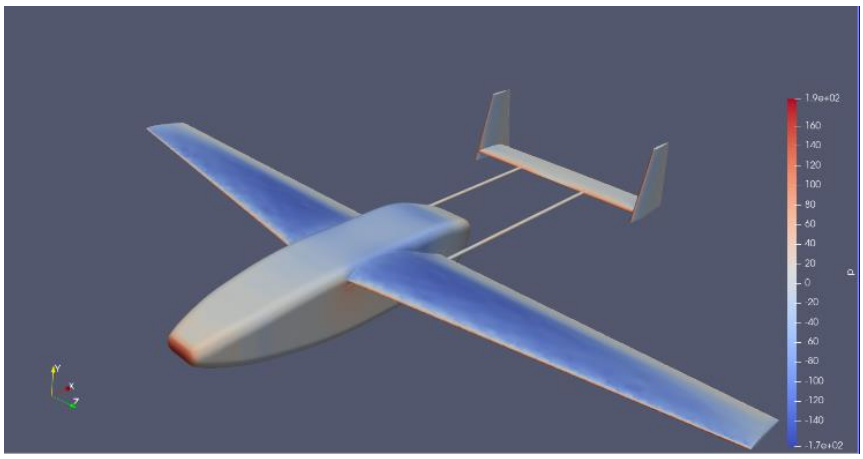

Fig. 13 Pressure plot at 0 deg AoA

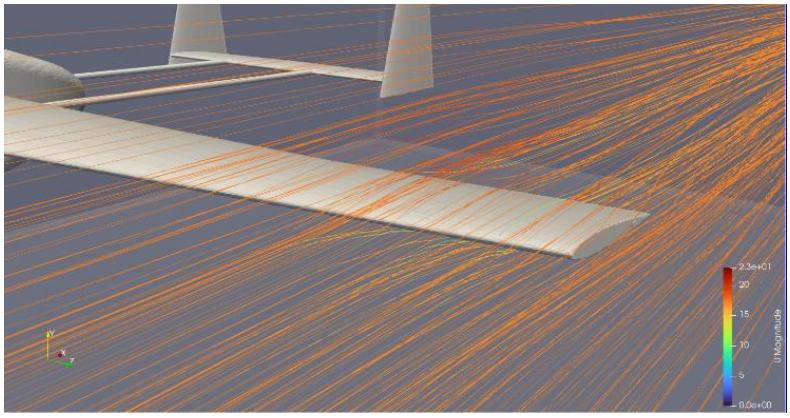

Fig. 14 Stream Lines at Wingtip at 0 deg AoA

From CFD data, a total Lift force of 22.8N was obtained at a cruise speed of 17m/s. The overall drag was estimated at around 3.95N.

4.3. Residuals:

The following plot given in Fig. 15 shows the Residuals for the CFD simulation, which converged at 10^-4.

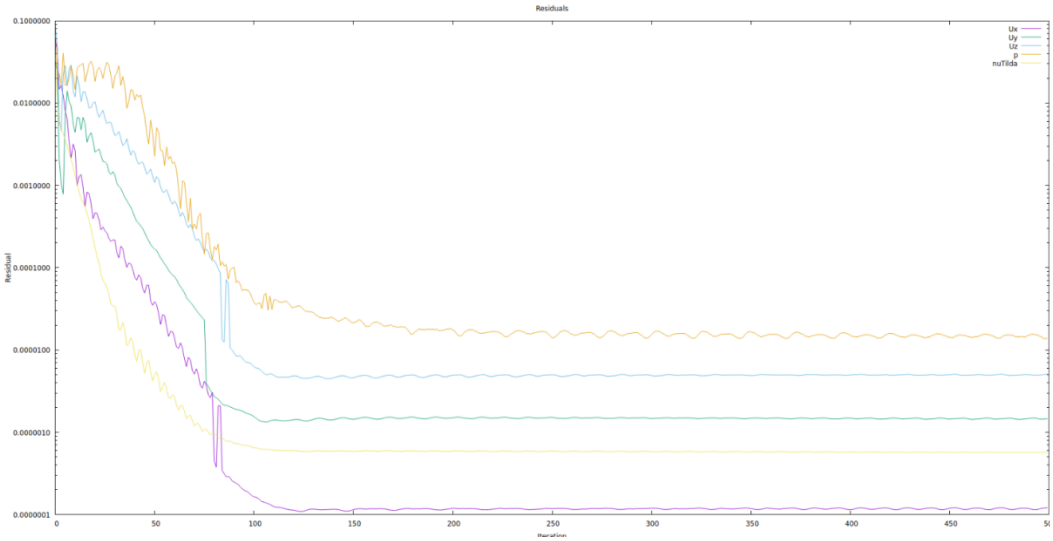

Fig. 15 Residual Plot

5. Structural design and material selection :

The structural design of a plane is a comprehensive and multifaceted method, necessitating a methodical and staged approach. Because of this reason, the Structure design for an aircraft has been divided into different stages here in our work. We are going to provide an in-depth expertise of the structural calculation methodologies and layout processes employed. Detailed structural designs and rigorous analysis may be addressed in the next studies. The design steps can be described in the given Flowchart in Fig. 16.

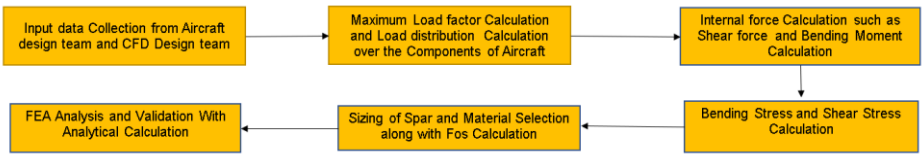

Fig. 16 Design Cycle for Structure Design of Aircraft

5.1 Load factor Calculation:

To start with the Load factor calculation, firstly the Input data from the aircraft design and CFD should be collected, and based on this input a V-n diagram is plotted. A V-n diagram is simply a graph plotted between the velocity and the maximum attainable load factor during normal flight conditions. It is also called a flight envelope as it guides us on what type of maneuvering can be obtained by the aircraft. Hence both the aerodynamic and structural limitation for a given airplane can be illustrated in the V-n diagram as given in

Fig. 17. There are two types of structural limitation on an aircraft i.e., Limit Load factor and Ultimate Load. Here Limit load factor is defined as the boundary associated with the permanent Structural Deformation of one or parts of an airplane, if 'n' is less than the limit load factor, the structure may deflect during a maneuver, but it will return to its original state when n = 1. If n is greater than the limit load factor, then the airplane structure will experience permanent deformation, and it will incur structural damage. Similarly, the ultimate load factor is the boundary associated with outright structural failure. Airplane parts will break if n exceeds the ultimate load factor [39]. Detailed information can be obtained by referring to the Aircraft Design and Performance book by JD Anderson[40]. The calculation of different Speeds is given in Table 8.

Table 8 Calculation of different Speeds

Point	Velocity Parameters	Load factor	Velocity(m/s)
A	Stall velocity	1	8.91
B	Corner Velocity	2.5	14.09
C	Max design cruise Speed	1.12	15
D	dive velocity	2	18
E	Inverted dive Speed	-1	18
F	Inverted corner Speed	-1	8.91

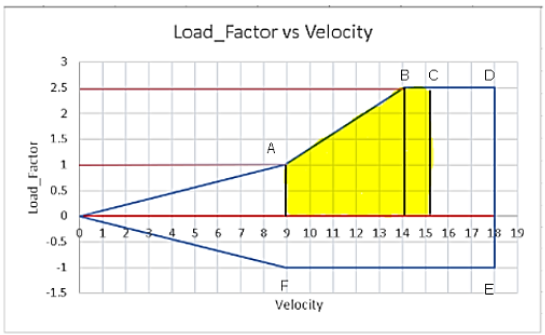

Fig. 17 V-n Diagram of aircraft

- Point A: The point indicates the stall velocity condition; stall velocity is defined as the minimum velocity condition at Cl_{imax}. The curve between 'o' and 'a' represents the maximum condition

$$V_{Stall}=\sqrt{\frac{2\times W\times g}{S\times C_{lmax}\times \rho}} \quad \textbf{(5)}$$

- Point B: The point indicates the Corner Speed; Corner Speed is also called maneuvering Speed. This is the speed of the aircraft during the level turn and the pull-up or pull-down maneuver.

$$V_{corner\ Speed}=\sqrt{\frac{2\times W\times g\times n_{max}}{S\times C_{lmax}\times \rho}} \quad \textbf{(6)}$$

- Point C: The point indicates the maximum design Cruise Speed. As we can see, the maximum design cruise Speed is also imposed by the curve BD which indicates the limit load factor on the aircraft. On cruise conditions, cl_{max} will be reduced to cl_{cruise}.

$$V_{cruise} = \sqrt{\frac{2 \times L}{\rho \times S \times Cl_{cruise}}} \quad \textbf{(7)}$$

- Point D: The point indicates the maximum attainable Speed by the aircraft. Beyond this velocity, the aircraft undergoes permanent deformation. The Curve 'DE' shows the maximum velocity attainable of aircraft. From Aircraft design and performance by Jd. Anderson [39] we got a relation between the dive Velocity and Cruise Velocity.

$$V_{dive\ Velocity} = 1.2 \times V_{cruise} \quad \textbf{(8)}$$

- The points 'E' and 'F' indicate the maximum load factor the aircraft can attain during the inverted flight. This is usually the Condition where the Cl is negative. This type of maneuvering is mainly done in military aircraft and is mostly restricted to aviation and UAVs. The yellow zone indicates the safest region for flying the UAV as in this the Structure will go through any permanent deformation and the performance of the overall UAV is also good for this reason.

After Plotting the V-n diagram, we get the maximum load factor from the V-n diagram. Here, In our case, we have a maximum load factor of 2.5. We have a fixed maximum load factor by following the [41] FAR.23 Regulations. After getting the maximum load factor, we will find our section-wise lift distribution. The section-wise lift distribution can be obtained by the CFD software. If the design is in the already stage, and the wing CFD is not available, then we can find out the Lift distribution using Schrenk's approximation [42]. In Table 9 below, we have calculated the lift distribution; we have divided the wing Semi Span into 8 different sections and after that; we have found the lift acting at each section and assumed that the lift will be acting at the local mean aerodynamic chord of the section. After obtaining the lift distribution, we multiplied the lift distribution with the maximum load factor and 1.5 'g' Condition to attain the maximum design load.

$$\text{Maximum design Load} = \textit{M}\text{ax. Load factor} \times 1.5 \quad \textbf{(9)}$$

As we have mentioned above the total wingspan is 1.328 m i.e., the wing Semi Span is 664 mm here we have divided the wing Semi Span into 8 sub-stations at 83 mm and then we locate the Centroid Station of each station where we are assuming the net lift for each section is acting.

Table 9 Lift Distribution vs Wing Semi-Span

Centroid Station	Lift distribution at Cruise Condition	Lift distribution at 4""(N)
41.5	1.57963	6.31852
124.5	1.50319	6.01276
207.5	1.36701	5.46804
290.5	1.19832	4.79328
373.5	0.986	3.944
456.5	0.758754	3.035016
539.5	0.49401	1.97604
622.5	0.248478	0.993912

From Table 9, above we can see the trend of lift distribution vs Station. This denotes an elliptical lift distribution, which means the maximum load will be acting at the root and as we move through the tip, the Load will decrease. As we obtained the lift distribution, we are now ready to find out the load acting on each spar. We are considering two circular tubes as a spar. Initially, we have assumed that the main Spar would be at 25% of the Chord length, the rear Spar would be at 60% of the Chord length and the Cp would be initially assumed at 45% now the reaction force on each spar will be found out by solving the moment balance.

After calculating the force distribution given in Table 10 on the frontal and the rear Spar now, we will calculate the shear force and bending Moment (as given in [43])acting on the Frontal and rear Spar given in Table 11. Here we are assuming at the tip the shear force and bending Moment will be zero and as we Move towards the root, the shear force and the bending moment will increase significantly. The formula for calculating the Shear force and bending moment is given below:

$$S.F_x = P + S.F_{(X-1)} \quad \textbf{(10)}$$

$S.F_x$= Shear force at Station 'x'.
P =Load acting between the Station ‘x’ and ‘'x-1’'.
$S.F_{X-1}$ = Shear force at Previous Station.

$$B.M_x = B.M_{(x-1)} + P \times \left(\frac{y}{2}\right) \quad \textbf{(11)}$$

$B.M_x$= Bending Moment at Station ‘x’.
P =Load acting between the Station ‘x’ and ‘x-1’.
M_{x-1} = Bending Moment at Previous Station.
$\left(\frac{y}{2}\right)$ = Half of the distance between the Span.

Table 10 Force distribution on Frontal and Rear Spar

Station	Force on frontal Spar	Force on the Rear Spar
41.5	2.707937143	3.610582857
124.5	2.576897143	3.435862857
207.5	2.343445714	3.124594286
290.5	2.054262857	2.739017143
373.5	1.690285714	2.253714286
456.5	1.300721143	1.734294857
539.5	0.8468742857	1.129165714
622.5	0.4259622857	0.5679497143

Table 11 Shear force and Bending Moment Calculation

Station	Shear Force (N) on frontal Spar	Bending Moment diagram on frontal Spar (N-mm)	Shear force on rear Spar (N)	Bending Moment on Rear Spar (N-mm)
0	13.946386	3463.3825	18.595182	4617.8434
83	11.238449	2418.2119	14.984599	3224.2825
166	8.661552	1592.3618	11.548736	2123.1491
249	6.3181063	970.70601	8.4241417	1294.2747
332	4.2638434	531.5551	5.6851246	708.74013
415	2.5735577	247.80295	3.4314103	330.40393
498	1.2728366	88.177587	1.6971154	117.57012

5.2 Material Selection:

As we can, the Load for our aircraft is very low, so we prefer the easily available carbon tubes that have good mechanical properties[44]. Instead of using ribs and stiffeners, we are using a San foam material for the overall wing. The mechanical properties of San foam can be taken from the [45]. The estimated weight for both the Wing will be around 240 grams by using the Material mentioned above.

5.3 Finite Element Analysis of the Wing:

By breaking complex systems down into smaller, more manageable components, a numerical approach called finite element analysis (FEA)[46] is used to analyze the structural behavior of the systems. Using Finite Element Analysis (FEA) [47] to analyze a wing can reveal information about its overall performance, stress distribution, and structural integrity. Here we are going to do the Static structural analysis of the wing and we will note down the total deformation and Von-misses Stress in the Wing at Maximum Loading Condition. A Computer-aided design is shown in Fig. 18 . We have used two Circular Spars and wing skins, ribs and stiffener have been avoided and solid wing skin has been made by San foam.

Fig. 18 Structure Design of Wing

5.4 Analysis Set-up:

In the analysis set-up, we will define the mesh Condition and the Boundary Condition. Both Meshing and Boundary Conditions play an important role in Solving any FEA analysis here we have defined the boundary Condition as a Static load of 40N acting in the Wing at 4g Condition and the fixed Support is given at the Root section. The default Meshing Parameters have been used for the Static Analysis test.

5.4.1. Static Analysis Result:

Here Fig. 19, Fig. 20, and Fig. 21 represent the Static analysis test of Wing. Here we have found out that at 4g Loading Condition, the maximum deformation in the Wing was 6 cm and the Average deformation was around 1.8 cm similarly the maximum Von-mises Stress for the wing is around 67.59 MPa, and the average stress in the overall wing 4.5 Mpa which justifies that the wing design can sustain the maximum Maneuvering Load Condition. The static analysis test gives the motivation to move ahead in the design. In future Work we can do the Composite analysis of the Wing and FSI [48] of the Wing can be done to predict the real lift behavior of the Wing and the Wing design can be optimized.

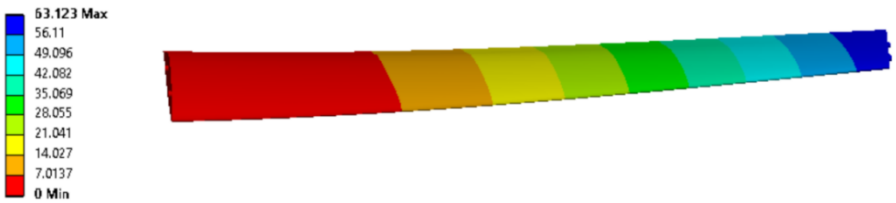

Fig. 19 Static deformation of Wing

Fig. 20 Von -Mises Stress on Wing Skin

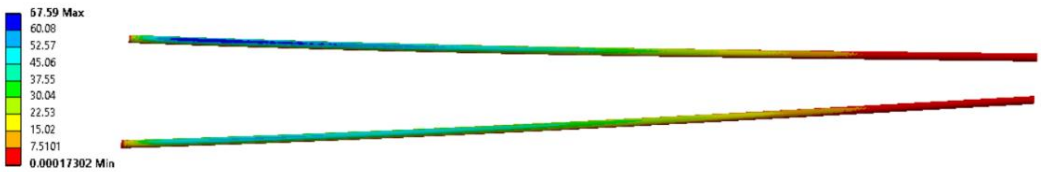

Fig. 21 Von-Mises Stress on Spar

6. Conclusion and Future Work:

The design process was initiated with design constraints, based on which parameters were calculated. OpenVSP was used for initial drag estimation, and fuselage shaping to house all the components.XFLR5 was employed for aerofoil selection and stability calculations to ensure the design is stable and efficient. OpenVSP exported the final CAD model for final aerodynamic simulation in OpenFOAM where CL and CD were calculated. This served as validation for the design's viability. Projected flight time exceeds 15 minutes with an approximate range of 15.3 kilometers at 17 meters per second cruise velocity. Before estimating this performance made preliminary calculations to select the motor.Our H-tail drone plan took shape through 3d printing, composite materials, and thermoplastics. It holded vital cargo within its body that was accessed quickly. Capable of delivering supplies to hard-to-reach areas during disasters, it had no landing gear and simply lands on its stomach as the carbon fiber body is tough enough to handle it. Flight distance varies around 20 km, based on battery and payload weight. Strong CFD/CAD tools helped us design this drone. Future work involves the prototype to be taken under extensive tests to improve its design with a 3D-printed model in a wind tunnel. This will test our fluid dynamics model's accuracy. Plus we plan in-depth studies on how fluid reacts with the drone's structure. This will help us understand how it performs better. Later versions of the drone might have landing gear for easier landing and take-off plus it could tweak the drone's design to carry more cargo. This would make it more useful for different situations. The design is not just about aiding in calamities. It can help with shipping goods, checking on Mother Nature, and farming tools. Its unique- style and tough build give it an edge. It can handle various tasks and the top-notch sensors and self-guiding systems will smooth out its workload and adaptability.

7. Acknowledgement :

We would like to express my deepest gratitude to our CollegeProfessor for their invaluable guidance and support throughout the process of writing this paper. Their insightful feedback, encouragement, and patience were instrumental in shaping the final version of this work. Without their expertise and dedication, this paper would not have been possible.We are profoundly thankful for their mentorship and the knowledge they have imparted to us.

References

1. *Munson, K.: Jane's unmanned aerial vehicles and targets. Jane's Information Group Limited (2000).*
2. *Mills, S.: The dawn of the drone: From the back-room boys of World War One. Casemate (2019).*
3. *Restas, A.: Drone applications for supporting disaster management. World Journal of Engineering and Technology. 3, 316–321 (2015).*
4. *Weisler, W., Stewart, W., Anderson, M.B., Peters, K.J., Gopalarathnam, A., Bryant, M.: Testing and characterization of a fixed-wing cross-domain unmanned vehicle operating in aerial and underwater environments. IEEE Journal of Oceanic Engineering. 43, 969–982 (2017).*
5. *Yuksek, B., Vuruskan, A., Ozdemir, U., Yukselen, M.A., Inalhan, G.: Transition Flight Modeling of a Fixed-Wing VTOL UAV. J Intell Robot Syst. 84, 83–105 (2016). https://doi.org/10.1007/s10846-015-0325-9.*
6. *Sadraey, M.H.: Aircraft design: A systems engineering approach. John Wiley & Sons (2012).*
7. *Mueller, T.J., DeLaurier, J.D.: A ERODYNAMICS OF S MALL V EHICLES. Annu. Rev. Fluid Mech. 35, 89–111 (2003). https://doi.org/10.1146/annurev.fluid.35.101101.161102.*
8. *Petricca, L., Ohlckers, P., Grinde, C.: Micro-and nano-air vehicles: State of the art. International journal of aerospace engineering. 2011, (2011).*
9. *Everaerts, J.: The use of unmanned aerial vehicles (UAVs) for remote sensing and mapping. The international archives of the photogrammetry, remote sensing, and spatial information sciences. 37, 1187–1192 (2008).*
10. *Clothier, R.A., Greer, D.A., Greer, D.G., Mehta, A.M.: Risk Perception and the Public Acceptance of Drones. Risk Analysis. 35, 1167–1183 (2015). https://doi.org/10.1111/risa.12330.*
11. *Nietz, T., Baber, S.: An Innovative UAV Design. In: AIAA 3rd "Unmanned Unlimited" Technical Conference, Workshop and Exhibit. American Institute of Aeronautics and Astronautics, Chicago, Illinois (2004). https://doi.org/10.2514/6.2004-6380.*
12. *Kedarisetty, S., Manathara, J.G.: Novel empirical models for estimating aerodynamic coefficients of small UAV propellers. AS. 6, 457–471 (2023). https://doi.org/10.1007/s42401-023-00203-y.*
13. *Vanlanduit, S., Sorgente, M., Zadeh, A.R., Güemes, A., Faisal, N.: Strain Monitoring. Structural Health Monitoring Damage Detection Systems for Aerospace. 219 (2021).*
14. *Austin, R.: Unmanned aircraft systems: UAVS design, development and deployment. John Wiley & Sons (2011).*
15. *Schroijen, M.J.T., Veldhuis, L.L.M., Slingerland, R.: Propeller Empennage Interaction Effects on the Vertical Tail Design of Multiengine Aircraft. Journal of Aircraft. 47, 1133–1140 (2010). https://doi.org/10.2514/1.46707.*
16. *Gomes, A.A.: Development of an UAV for the Air Cargo Challenge 2017 Competition, https://search.proquest.com/openview/546d65a2842c57183f5879d39af2f77a/1?pq-origsite=gscholar&cbl=2026366&diss=y, (2017).*
17. *Hieu, N.K., Loc, H.T.: Airfoil Selection for Fixed Wing of Small Unmanned Aerial Vehicles. In: Duy, V.H., Dao, T.T., Zelinka, I., Choi, H.-S., and Chadli, M. (eds.) AETA 2015: Recent Advances in Electrical Engineering and Related Sciences. pp. 881–890. Springer International Publishing, Cham (2016). https://doi.org/10.1007/978-3-319-27247-4_73.*
18. *Li, Z., Wang, D.: Analysis and experimental study on different airfoils in heavy unmanned aerial vehicle. AS. 4, 37–48 (2021). https://doi.org/10.1007/s42401-020-00072-9.*
19. *Kapoulas, I.K., Statharas, J.C., Hatziefremidis, A., Baldoukas, A.K.: Fast Airfoil Selection Methodology for Small Unmanned Aerial Vehicles. Applied Sciences. 12, 9328 (2022).*
20. *Strelets, D., Parkhaev, E., Fevralskikh, A., Gueraiche, D., Das, D.: Airfoil optimization methodology and CFD validation for Mars atmospheric conditions. AS. 6, 175–186 (2023). https://doi.org/10.1007/s42401-022-00181-7.*
21. *Priyanka, R., Sivapragasam, M., Narahari, H.K.: Multi-fidelity Aerodynamic Optimization of an Airfoil at a Transitional Low Reynolds Number. In: Kumar, S.K., Narayanaswamy, I., and Ramesh, V. (eds.) Design and Development of Aerospace Vehicles and Propulsion Systems. pp. 239–252. Springer, Singapore (2021). https://doi.org/10.1007/978-981-15-9601-8_18.*
22. *Kumar, M., Sunil, G.K., Shanmugam, V., Balu, G.: Hinge Moment Characterization of All Movable Control Surface. In: Kumar, S.K., Narayanaswamy, I., and Ramesh, V. (eds.) Design and Development of Aerospace Vehicles and Propulsion Systems. pp. 185–196. Springer Singapore, Singapore (2021). https://doi.org/10.1007/978-981-15-9601-8_13.*
23. *Sulistyo, M.E., Ramadhan, M.I.A., Inderawan, A.P.S.: AERODYNAMIC CHARACTERISTIC AND AIRPLANE STABILITY AT THE PLERIMENARY DESIGN STAGE. Journal of Electrical, Electronic, Information, and Communication Technology. 2, 18–20.*
24. *McDonald, R.A.: Advanced Modeling in OpenVSP. In: 16th AIAA Aviation Technology, Integration, and Operations Conference. American Institute of Aeronautics and Astronautics, Washington, D.C. (2016). https://doi.org/10.2514/6.2016-3282.*
25. *Segui, M., Botez, R.M.: Aerodynamic coefficients prediction from minimum computation combinations using OpenVSP software. International Journal of Mechanical and Industrial Engineering. 12, 9–16 (2018).*
26. *xflr5, https://www.xflr5.tech/xflr5.htm, last accessed 2024/04/24.*
27. *Roskam, J.: Airplane flight dynamics and automatic flight controls. DARcorporation (1998).*

28. *Kurukularachchi, P.L., Munasinghe, S.R., De Silva, H.: Stability analysis for a twin boom H-tail Medium Scale UAV through simulated dynamic model. In: 2016 Moratuwa Engineering Research Conference (MERCon). pp. 415–420. IEEE (2016).*
29. *Mieloszyk, J., Tarnowski, A., Tomaszewski, A., Goetzendorf-Grabowski, T.: Validation of flight dynamic stability optimization constraints with flight tests. Aerospace Science and Technology. 106, 106193 (2020).*
30. *Mi, B., Zhan, H.: Review of Numerical Simulations on Aircraft Dynamic Stability Derivatives. Arch Computat Methods Eng. 27, 1515–1544 (2020). https://doi.org/10.1007/s11831-019-09370-8.*
31. *Robertson, E., Choudhury, V., Bhushan, S., Walters, D.K.: Validation of OpenFOAM numerical methods and turbulence models for incompressible bluff body flows. Computers & Fluids. 123, 122–145 (2015).*
32. *Medina, H., Beechook, A., Saul, J., Porter, S., Aleksandrova, S., Benjamin, S.: Open source computational fluid dynamics using OpenFOAM. In: Royal Aeronautical Society, General Aviation Conference, London (2015).*
33. *OpenFOAM v9 User Guide - Index, https://doc.cfd.direct/openfoam/user-guide-v9/bookindex, last accessed 2024/03/16.*
34. *Karman, S.L., Wyman, N.J.: Automatic Unstructured Mesh Generation with Geometry Attribution. In: AIAA Scitech 2019 Forum. American Institute of Aeronautics and Astronautics, San Diego, California (2019). https://doi.org/10.2514/6.2019-1721.*
35. *Shafer, T., Viken, S., Favaregh, N.M., Zeune, C.H., Williams, N., Dansie, J.: Comparison of Computational Approaches for Rapid Aerodynamic Assessment of Small UAVs. In: 52nd Aerospace Sciences Meeting. American Institute of Aeronautics and Astronautics, National Harbor, Maryland (2014). https://doi.org/10.2514/6.2014-0039.*
36. *Lift Coefficient, https://www1.grc.nasa.gov/beginners-guide-to-aeronautics/lift-coefficient/, last accessed 2024/03/16.*
37. *The Drag Coefficient, https://www.grc.nasa.gov/www/k-12/VirtualAero/BottleRocket/airplane/dragco.html, last accessed 2024/03/16.*
38. *Hövelmann, A., Breitsamter, C.: Aerodynamic characteristics of the sagitta diamond wing demonstrator configuration. In: DGLR Kongress (2012).*
39. *Anderson, J.: EBOOK: Fundamentals of Aerodynamics (SI units). McGraw hill (2011).*
40. *Anderson Jr, J.D.: mance. (1999).*
41. *Mazhar, F., Khan, A.: Structural Design of a UAV Wing Using Finite Element Method. In: 51st AIAA/ASME/ASCE/AHS/ASC Structures, Structural Dynamics, and Materials Conference
 18th AIAA/ASME/AHS Adaptive Structures Conference
 12th. American Institute of Aeronautics and Astronautics, Orlando, Florida (2010). https://doi.org/10.2514/6.2010-3099.*
42. *Putra, C.A., Julistina, R., Moelyadi, M.A., Mulyanto, T.: Comparative study between Schrenk and CFD analysis for predicting lift distribution along wing span of glider aircraft. Advance in Aerospace Science and Technology in Indonesia. 1, 108–117 (2016).*
43. *Megson, T.H.G.: Aircraft structures for engineering students. Butterworth-Heinemann (2016).*
44. *GIBSON, L.J.: Cellular materials: Structure, properties, and applications. In: Frontiers of Engineering: Reports on Leading Edge Engineering from the 1996 NAE Symposium on Frontiers of Engineering. p. 75. National Academies Press (1997).*
45. *Basri, E.I., Mustapha, F., Sultan, M.T.H., Basri, A.A., Abas, M.F., Majid, M.S.A., Ahmad, K.A.: Conceptual design and simulation validation based finite element optimisation for tubercle leading edge composite wing of an unmanned aerial vehicle. Journal of Materials Research and Technology. 8, 4374–4386 (2019).*
46. *DS, C.R.M., Plesha, M.E., Witt, R.J.: Concepts and applications of finite element analysis, (1989).*
47. *Aabid, A., Zakuan, M.A.M.B.M., Khan, S.A., Ibrahim, Y.E.: Structural analysis of three-dimensional wings using finite element method. AS. 5, 47–63 (2022). https://doi.org/10.1007/s42401-021-00114-w.*
48. *Criollo, L., Sánchez Sánchez, X., Abatta-Jácome, L., Haro, E.E.: Finite Element Simulation of Aircraft Wing with Fluid-Structure Interaction. In: Botto-Tobar, M., Cruz, H., and Diaz Cadena, A. (eds.) Recent Advances in Electrical Engineering, Electronics and Energy. pp. 31–43. Springer International Publishing, Cham (2022). https://doi.org/10.1007/978-3-031-08288-7_3.*
49. *Kohar, Nikhil & Chaudhary, Pramod & Bishwakarma, Sunil & Karthik, K.. (2022). DESIGN AND ANALYSIS OF SMALL-SCALE DIFFERENT TYPES OF AIRCRAFT STRUCTURES 1 Nikhil kohar. YMER Digital. 21. 13.*